ChemComm

COMMUNICATION

View Article Online
View Journal | View Issue

Cite this: *Chem. Commun.*, 2022, **58**, 2524

Received 23rd November 2021,
Accepted 14th January 2022

DOI: 10.1039/d1cc06596c

rsc.li/chemcomm

Bisulfate as a redox-active ligand in vanadium-based electrocatalysis for CH_4 functionalization†

Danlei Xiang,‡[a] Sheng-Chih Lin,‡[b] Jiao Deng,[a] Hao Ming Chen *[b] and Chong Liu *[ac]

The roles of unforgiving H_2SO_4 solvent in CH_4 activation with molecular catalysts have not been experimentally well-illustrated despite computational predictions. Here, we provide experimental evidence that metal-bound bisulfate ligand introduced by H_2SO_4 solvent is redox-active in vanadium-based electrocatalytic CH_4 activation discovered recently. Replacing one of the two terminal bisulfate ligands with redox-inert dihydrogen phosphate in the pre-catalyst vanadium (V)-oxo dimer completely quenches its activity towards CH_4, which may inspire environmentally benign catalysis with minimal use of H_2SO_4.

Abundance of CH_4 welcomes sustainable methods of converting CH_4 into fuels or commodity chemicals such as CH_3OH at low temperatures.[1] Since the existing two-step industrial route of CH_4-to-CH_3OH conversion is capital-intensive and operates under high temperatures and pressures,[2] direct activation and two-electron oxidation of CH_4 with molecular transition-metal-based catalysts offers an alternative. In those systems, concentrated sulfuric acid (98% H_2SO_4) or even oleum ($H_2SO_4{\cdot}xSO_3$)[1c,3] are frequently applied as solvent in homogenous[4] and electrochemical catalysis[5] in order to mitigate undesirable further oxidation, thanks to the formation of oxidatively stable methyl bisulfate (CH_3OSO_3H),[6] a precursor of CH_3OH, as the product of two-electron oxidation of CH_4. Yet, it is proposed computationally that there are additional roles of H_2SO_4 solvent in the critical step of homogeneous Au^{III}, Pd^{II}, Hg^{II}, and Sb^{V}-based CH_4 activation[7]—metal-bound bisulfate ligands ($-OSO_3H$) undergo an intramolecular abstraction of a proton from CH_4 concurrent with formation of a metal–CH_3 bond (Fig. S1, ESI†).

Other roles of bisulfate ligand are suggested in electrocatalytic CH_4 activation in H_2SO_4. We previously reported room-temperature electrochemical CH_4 functionalization into CH_3OSO_3H in 98% H_2SO_4 with molecular catalyst vanadium (V)-oxo dimer $V_2^{V,V}$ (**1** in Fig. 1).[5c] Kinetics suggests preceding CH_4 activation, there exists a turnover-limiting electrochemical oxidation of d^0 $V_2^{V,V}$ into a CH_4-reactive cation radical $V_2^{V,V+}$, which is computationally predicted to be an oxygen radical mostly localized on monodentate bisulfate ligand (Fig. 1a). Moreover, it is computationally suggested that CH_4 activation on an electrochemically generated $Pd_2^{III,III}$ dimer is initiated on metal-bound bisulfate *via* an H-atom abstraction

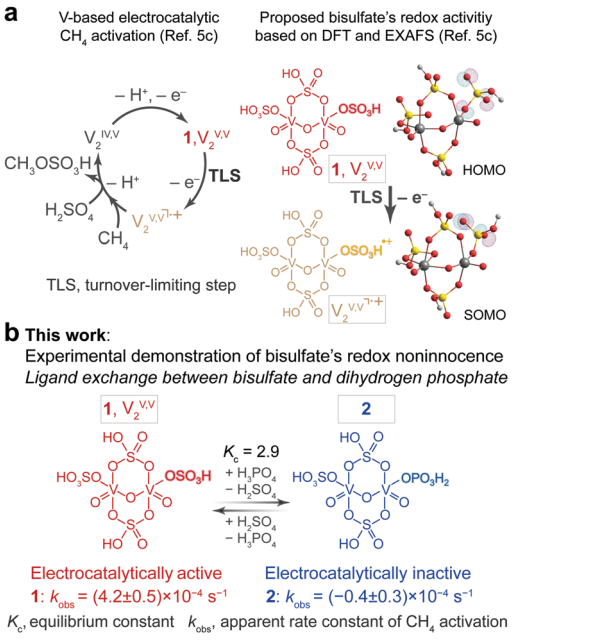

Fig. 1 (a) Proposed mechanism of CH_4 functionalization initiated by the electrochemically generated cation radical ($V_2^{V,V\bullet+}$) from a vanadium (V)-oxo dimer (**1**, $V_2^{V,V}$, based on DFT and EXAFS results).[5c] (b) Mono-substitution of bisulfate with a dihydrogen phosphate ligand leads to electrocatalytically inactive **2** in H_2SO_4–H_3PO_4 mixed solvent.

[a] *Department of Chemistry and Biochemistry, University of California Los Angeles, Los Angeles, California 90095, USA. E-mail: chongliu@chem.ucla.edu*
[b] *Department of Chemistry, National Taiwan University, Taipei 10617, Taiwan. E-mail: haomingchen@ntu.edu.tw*
[c] *California NanoSystems Institute, University of California Los Angeles, Los Angeles, California 90095, USA*

† Electronic supplementary information (ESI) available: Full experimental details, data analysis and additional figures. See DOI: 10.1039/d1cc06596c

‡ Danlei Xiang and Sheng-Chih Lin have equally contributed to this work.

process (Fig. S1, ESI†),[8] which similarly hints at a redox-active bisulfate ligand with an O radical. Such insights suggest the bisulfate ligand and hence H_2SO_4 solvent is critical towards the observed activities in homogenous and electrochemically catalytic systems. However, experimental evidence remains elusive. A deeper understanding about H_2SO_4 and bisulfate ligand's role in CH_4-activating catalytic cycle will help us to design environmentally benign catalytic systems with minimal use of 98% H_2SO_4 while yielding CH_3OH or its equivalent without excessive oxidation.

Here, we seek to experimentally validate the redox noninnocence of bisulfate ligand in the context of searching for an alternative electrolyte other than unforgiving H_2SO_4. Because the formal oxidation state of vanadium (V) metal centers cannot be further increased, electrocatalytic CH_4 activation based on $V_2^{V,V}$ pre-catalyst[5c] (Fig. 1) is selected as a model system devoid of the potential interference from metal-based redox changes. We hypothesize substituting the monodentate bisulfate ligand with a more redox-inert dihydrogen phosphate moiety ($-OPO_3H_2$),[9] by partly replacing H_2SO_4 solvent with H_3PO_4, is an effective perturbation of the catalytic center and a venue to probe the role of bisulfate ligand (Fig. 1b).

We observed a chemical equilibrium between $V_2^{V,V}$ (**1**) and the variant mono-substituted by a dihydrogen phosphate ligand (**2**) in mixtures of H_3PO_4 and H_2SO_4. UV-Vis spectrometry was conducted when V_2O_5 was dissolved in H_3PO_4–H_2SO_4 electrolytes of different molar concentration ratios c_{H3PO4}/c_{H2SO4} (Fig. S2a, ESI†). A symmetric bimodal distribution of the absorption peaks with an isosbestic point at 309 nm was observed when the total vanadium concentration C_V = 0.4 mM (Fig. 2a). In 98% H_2SO_4 (*i.e.* c_{H3PO4}/c_{H2SO4} = 0/18.0), the strong absorption peak at λ_{max} = 329 nm is assigned to LMCT band of **1**.[5c,10] With the introduction of H_3PO_4 solvent and hence the dihydrogen phosphate ligand, an isosbestic point in Fig. 2a suggests only one new species **2** at λ_{max} = 291 nm formed at the expense of **1**. The blue-shifted LMCT band in **2** indicates **2** contains a larger energy gap of LMCT and less oxidatively accessible ligand-based molecular orbitals given the same d^0 vanadium (V) metal centers in **1** and **2**.[11] Such a stabilization of the ligand-like molecular orbitals is consistent with presumed ligand substitution by redox-inert dihydrogen phosphate.[12] Taking advantage of the isosbestic point,[13] we established a model to determine the equilibrium constant between **1** and **2** (K_c) and number of bisulfate ligands substituted by dihydrogen phosphate (n),

$$\mathbf{1} + n\mathrm{H_3PO_4} \leftrightarrow \mathbf{2} + n\mathrm{H_2SO_4} \quad K_c = \frac{[\mathbf{2}]^1 c_{\mathrm{H_2SO_4}}{}^n}{[\mathbf{1}]^1 c_{\mathrm{H_3PO_4}}{}^n} \qquad (1)$$

$$\log_{10}\left(\frac{[\mathbf{1}]}{[\mathbf{2}]}\right) = -\log_{10}(K_c) + n\log_{10}\left(\frac{c_{\mathrm{H_2SO_4}}}{c_{\mathrm{H_3PO_4}}}\right) \qquad (2)$$

In a mixed solvent of a specific c_{H3PO4}/c_{H2SO4} value, the absorbances at 329 nm and 291 nm depend on the concentrations of **1** and **2** ([**1**] and [**2**], respectively), as well as their molar extinction coefficients at 329 nm and 291 nm. Analysis of Fig. 2a yields values of [**1**] and [**2**] at different c_{H3PO4}/c_{H2SO4} (Fig. 2b and Table S1, ESI†). When c_{H3PO4}/c_{H2SO4} > 4.7/13.5, biphosphate-substituted **2** becomes predominant. Following eqn (2), plotting $\log_{10}([\mathbf{1}]/[\mathbf{2}])$ against $\log_{10}(c_{H2SO4}/c_{H3PO4})$ yields a linear relationship (Fig. 2c) with its slope and y-intercept corresponding to n and $-\log_{10}(K_c)$, respectively. As n = 1.18 and K_c = 2.9 from Fig. 2c (ESI†), an equilibrated mono-substitution of bisulfate ligand with dihydrogen phosphate between **1** and **2** is established.

X-Ray absorption spectroscopy suggests mono-substitution occurs on the terminal bisulfate ligand. Two vanadium solutions with c_{H3PO4}/c_{H2SO4} = 3.5/14.6 and 7.0/11.3 were measured with C_V = 10 mM. In the results of XANES spectra for vanadium atoms, the sample of c_{H3PO4}/c_{H2SO4} = 7.0/11.3 displayed a slight higher formal oxidation state of the vanadium center than the one of c_{H3PO4}/c_{H2SO4} = 3.5/14.6, which is consistent with the substitution of a less oxidatively accessible $-OPO_3H_2$ that shifts the rising-edge and edge maxima of vanadium atoms to higher energy regions (Fig. S2a and b, ESI†). Fig. 2d shows the EXAFS spectra for samples with c_{H3PO4}/c_{H2SO4} = 3.5/14.6 (yellow trace) and 7.0/11.3 (blue trace), mixtures of **1** and **2** with molar ratios quantifiable from Fig. 2b. Fig. 2e shows the average fitting results from EXAFS based on the coexistence of **1** and **2**. In the first coordination shell near the metal, there are five V-bound O atoms with three different V–O bond lengths (Fig. 2d, blue area). The second shell (Fig. 2d, >2.0 Å, green area) includes the other V atom in the dimer structure and two S atoms from two bridging bisulfates; more importantly, there are S or P atoms less than one equivalent from the non-bridging $-OSO_3H$ or $-OPO_3H_2$ moiety (V–S and V–P, respectively, with a subscript "a" in Fig. 2e) and the averaged coordination numbers of the terminal $-OSO_3H$ and $-OPO_3H_2$ add up to one equivalent in both samples. This suggests the mono-substitution observed from UV-Vis in Fig. 2a corresponds to the replacement of one non-bridging bisulfate ligand with dihydrogen phosphate. On average, the ratios of the coordination numbers of the non-

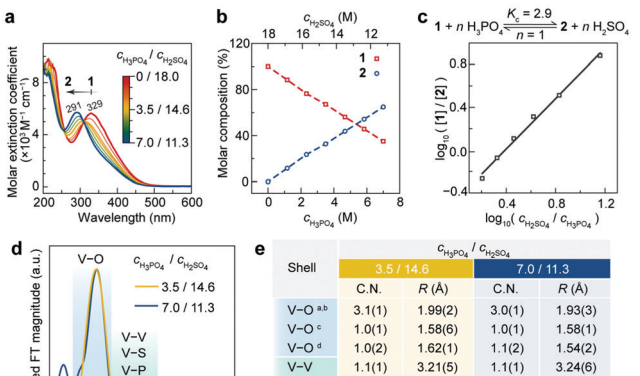

Fig. 2 (a) UV-Vis spectra in different H_2SO_4–H_3PO_4 mixed solvents. C_V = 0.4 mM. (b) The molar composition of **1** and **2** as a function of solvent composition. (c) The logarithms of the concentration ratios between **1** and **2**, $\log_{10}([\mathbf{1}]/[\mathbf{2}])$, against the logarithms of the concentration ratios between H_2SO_4 and H_3PO_4, $\log_{10}(c_{H2SO4}/c_{H3PO4})$. (d and e) EXAFS measurements (d) and structural optimization (e) for the vanadium (V)-oxo species in two representative electrolytes (c_{H3PO4}/c_{H2SO4} = 3.5/14.6 and 7.0/11.3). C_V = 10 mM.

bridging terminal –OSO_3H and –OPO_3H_2 ligand ($C.N._{V-S}/C.N._{V-P}$) from EXAFS are quite comparable with the expected ratios obtained from UV-Vis in Fig. 2b (Table S2, ESI†), corroborating the mono-substitution on terminal bisulfate ligand (Fig. 1b) and offering a suitable perturbation to the electrocatalyst to study the role of terminal –OSO_3H ligand.

The activities of electrocatalytic CH_4 functionalization in H_3PO_4–H_2SO_4 mixed electrolyte were observed to decrease with the increase of c_{H3PO4}/c_{H2SO4} value, and hence the percentage of **2** in the solution. Representative cyclic voltammograms (CVs) in atmospheric N_2 (Fig. 3a and Fig. S3, ESI†) and CH_4 (Fig. 3b and Fig. S4, ESI†) of C_V = 10 mM were recorded at varying scan rates in H_3PO_4–H_2SO_4 electrolytes with a 2 mm diameter Pt working electrode, and all following potentials are reported with respect to Hg_2SO_4/Hg. The vanadium V/IV redox couple was consistently at ~0.64 V. The generation of cation radical $V_2^{V,V\bullet+}$ *via* one-electron oxidation presumably from terminal –OSO_3H (noted as TLS in Fig. 1a)[5c] was observed beyond 1.4 V. In general, introduction of H_3PO_4 electrolyte suppresses or anodically shifts oxidation current for the formation of a cation radical and decreases the difference of oxidation current in N_2 and CH_4 when $E > 1.4$ V (Fig. 3a and b). Such observations reinforce mono-substituting one redox-active terminal bisulfate in **1** with redox-inactive dihydrogen phosphate in **2** leads to a more oxidatively demanding electrogeneration of the CH_4-reactive cation radical and a smaller electrocatalytic current density in CH_4. Our investigation continued with bulk electrolysis under 1 bar CH_4 with C_V = 10 mM in H_3PO_4–H_2SO_4 electrolyte when E = 1.75 to 2.45 V with an FTO working electrode (Fig. S5, ESI†). CH_3OSO_3H was the only product observed in the liquid phase (Fig. S6, ESI†). Faradaic efficiency (FE) and partial current density of CH_4 oxidation to CH_3OSO_3H (j_{CH4}) were recorded in Fig. 3c and d. At small E values, CH_4 activation seemed to be kinetically controlled and increased with larger E until $E > 2.25$ V when other limiting factors including mass transport surfaced. While optimal values of FE and j_{CH4} were achieved at *ca.* 2.2 V, electrolytes of larger c_{H3PO4}/c_{H2SO4} lead to lower values of FE and j_{CH4}, consistent with the presumed lower redox activities incurred by dihydrogen phosphate substitution. More strikingly, Tafel analysis by plotting $\log_{10}(j_{CH4})$ *versus* E leads to different values of Tafel slopes in different H_3PO_4–H_2SO_4 mixtures. In Fig. 3e, when [**1**]/[**2**] ratios correspond to 100/0 and 67/33 (Table S1, ESI† c_{H3PO4}/c_{H2SO4} = 0/18.0 (red) and 3.5/14.6 (yellow), respectively), nearly overlapping data points were recorded when $E < 2.1$ V with Tafel slopes of 116 and 114 mV/dec, respectively. While their differences at $E > 2.1$ V may be indicative of the differences in [**1**]/[**2**] ratios, the similar if not the same Tafel slopes of about 120 mV dec^{-1} indicate the same turnover-limiting step (TLS) of electron transfer (E step),[14] which is presumed to be the first electrochemical oxidation of **1** into cation radical $V_2^{V,V\bullet+}$ with a redox-active terminal bisulfate ligand as reported before (step TLS in Fig. 1a).[5c] The same values of Tafel slopes at c_{H3PO4}/c_{H2SO4} = 0/18.0 and 3.5/14.6 also suggest H_2SO_4 molecule does not participate in TLS and the TLS is independent of H_2SO_4 concentration. However, a Tafel slope of 188 mV dec^{-1} was observed (blue in Fig. 3e) when c_{H3PO4}/c_{H2SO4} = 7.0/11.3 and [**1**]/[**2**] ratio is 35/65 (Table S1, ESI†). Such a Tafel slope much larger than 120 mV dec^{-1} indicates a TLS of chemical reaction (C step) preceding any electrochemical charge transfers.[14] This observation also excludes a possible shift of TLS to the step of CH_4 activation after formation of $V_2^{V,V\bullet+}$, because a turnover-limiting chemical step of CH_4 activation (C step) in an EC′ mechanism would have led to a smaller Tafel slope[14] that is not what we have observed experimentally. At high c_{H3PO4}/c_{H2SO4} values, a pre-equilibrium between **1** and **2** exists due to the predominance of **2** (Fig. 1b) and a C step converting **2** into **1** becomes turnover-limiting before electrochemical oxidation of **1** into CH_4-reactive $V_2^{V,V\bullet+}$.

Analysis of the pseudo-first-order apparent rate constant k_{obs} of CH_4 electrocatalysis at different values of c_{H3PO4}/c_{H2SO4} supports the hypothesized redox inactivity of **2** and that only **1** is directly electrochemically oxidizable to yield CH_4-reactive cation radical $V_2^{V,V\bullet+}$. At E = 2.25 V, j_{CH4} was obtained at different values of c_{H3PO4}/c_{H2SO4} (Fig. 3f). The average values of k_{obs} based on C_V were determined from the diffusion coefficient of vanadium (V)-oxo dimer at different values of c_{H3PO4}/c_{H2SO4} (Fig. S7 and Table S3, ESI†).[15] Fig. 3g depicts k_{obs} as a function of c_{H3PO4} and c_{H2SO4}. In Fig. 3f and g, the average activities of CH_4 activation decrease with increasing c_{H3PO4} under the same C_V. The 4.3-fold and 3.9-fold changes of j_{CH4} (Fig. 3f) and k_{obs} (Fig. 3g), respectively, under a 1.6-fold decrease of c_{H2SO4} suggest the observed changes of j_{CH4} and

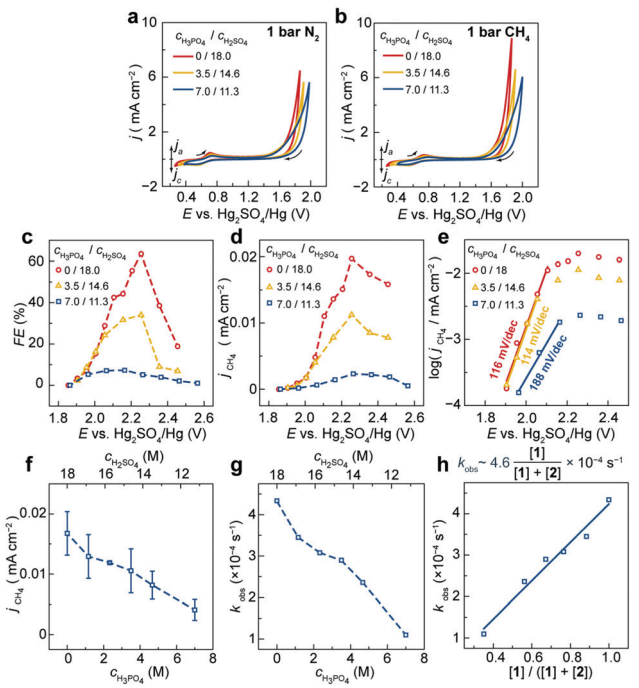

Fig. 3 (a and b) CVs in 1 bar N_2 (a) and CH_4 (b) 100 mV s^{-1}. (c–e) Faradaic efficiencies (c) and partial current densities (d) and the Tafel plots (e) measured at different potentials. (f–h) Partitioning the reactivities between **1** and its dihydrogen–phosphate-substituted variant **2**, E = 2.25 V. (f and g) Partial current densities (f) and apparent rate constants (g) as a function of the composition in H_3PO_4–H_2SO_4 mixed electrolyte. (h) The relationship between the apparent rate constants and molar composition of **1**. Each data point shows the average of three individual measurements. C_V = 10 mM.

k_{obs} do not directly originate from the change of TLS's kinetic rate that might have been a function of c_{H2SO4}, because Tafel slope analysis suggests H_2SO_4 molecule does not participate in turnover-limiting one-electron oxidation of $V_2^{V,V}$. We further plotted k_{obs} as a function of the percentage of **1** in the mixture of **1** and **2**, [**1**]/([**1**] + [**2**]), under different values of c_{H3PO4}/c_{H2SO4} at C_V = 10 mM (Fig. 3h). A linear relationship was observed and extrapolation of this linear relationship yields $k_{obs} = (4.2 \pm 0.5) \times 10^{-4}$ and $(-0.4 \pm 0.3) \times 10^{-4}$ s^{-1} when [**1**]/([**1**] + [**2**]) = 1.0 (pure **1**) and 0.0 (pure **2**), respectively. The difference of calculated k_{obs} between **1** and **2** quantitatively confirms only **1** is electrochemically oxidizable to a CH_4-reactive cation radical and **2** is redox-innocent at E = 2.25 V. It is intriguing that replacing only one of the two terminal $-OSO_3H$ moieties in **1** with $-OPO_3H_2$ leads to such a dramatic difference of k_{obs} between **1** and **2**. Although the electrochemically generated cation radical $V_2^{V,V\bullet+}$ is computationally considered as a radical localized on the terminal oxygen atom of monodentate bisulfate ligand (Fig. 1a),[5c] our results hint the singly occupied molecular orbital (SOMO) of $V_2^{V,V\bullet+}$ is highly delocalized across the vanadium (V)-oxo dimer. A $-OPO_3H_2$ moiety away from the formally electrooxidized $-OSO_3H$ has an impact on energetics of electrogenerated cation radical. Such results are indeed supportive of the computational results of the electrochemically generated $Pd_2^{III,III}$ dimer in H_2SO_4.[8] Thanks to the covalent nature of Pd–O bond and possible formation of delocalized biradicals, two equally viable CH_4-activation pathways were proposed for the $Pd_2^{III,III}$ dimer and both include the step of H-atom abstraction from CH_4 initiated by an O atom in metal-bound bisulfate ligand (Fig. S1, ESI†).[8] In our work, because the pre-catalyst **1** has already been at vanadium's highest formal oxidation state that precludes any metal-based oxidation and metalloradical formation, our experiments provide clear evidence that bisulfate is redox-active during electrocatalytic CH_4 activation. Given similar electrochemical driving forces between vanadium-based electrocatalysis and others,[5a,b,16] one working hypothesis is the redox noninnocence of metal-bound bisulfate is universally present in electrocatalytic CH_4 activation in H_2SO_4-based electrolyte. Indeed, the universal reactivities of electrocatalytic CH_4 functionalization across early transition metals (Group 4 to 6, Period 4 to 6) reported by our group recently offer additional support towards our argument.[16] While we do not have enough information to extend such a hypothesis for homogenous CH_4 functionalization in H_2SO_4 or oleum through electrophilic activation,[7a–d] we contend redox activity of metal-bound bisulfate should be considered during the mechanistic investigation.

Our results offer a reminder in the context of translating electrocatalysis of CH_4 activation in currently prevailing yet unfriendly H_2SO_4 solvent[17] to a more benign electrolyte. Removal of H_2SO_4 solvent not only destabilizes CH_3OH or its equivalent as the two-electron oxidation product[6] but also may inadvertently remove the electrocatalytic active species important towards activating CH_4 and alter the overall reaction mechanism. Designing a bisulfate-rich microenvironment for electrocatalytic active sites with minimal H_2SO_4 usage could be a possible route to keep the electrocatalytic mechanism and activity of CH_4 functionalization with least infrastructure reliance and environmental footprints.

H. M. C. acknowledges Ministry of Science and Technology, Taiwan (Contract no. MOST 107-2628-M-002015-RSP). C. L. acknowledges NSF Award (CHE-1955836), and startup fund from University of California, Los Angeles.

Conflicts of interest

There are no conflicts to declare.

Notes and references

1 (*a*) E. J. Dlugokencky and P. Bousquet, *Science*, 2014, **343**, 493–495; (*b*) D. Malakoff, *Science*, 2014, **344**, 1464–1467; (*c*) N. J. Gunsalus, A. Koppaka, S. H. Park, S. M. Bischof, B. G. Hashiguchi and R. A. Periana, *Chem. Rev.*, 2017, **117**, 8521–8573; (*d*) O. Edenhofer, *et al.*, *Working Group III Contribution to the Fifth Assessment Report of the Intergovernmental Panel on Climate Change, Climate Change 2014: Mitigation of Climate Change*, Cambridge University Press, 2015.
2 J. Rostrup-Nielsen and L. J. Christiansen, *Concepts in Syngas Manufacture*, Imperial College Press, 2011.
3 (*a*) M. Ravi, M. Ranocchiari and J. A. van Bokhoven, *Angew. Chem., Int. Ed.*, 2017, **56**, 16464–16483; (*b*) X. Meng, X. Cui, N. P. Rajan, L. Yu, D. Deng and X. Bao, *Chem*, 2019, **5**, 2296–2325.
4 (*a*) R. A. Periana, D. J. Taube, S. Gamble, H. Taube, T. Satoh and H. Fujii, *Science*, 1998, **280**, 560–564; (*b*) R. A. Periana, *et al.*, *Science*, 1993, **259**, 340–343; (*c*) N. Basickes, T. E. Hogan and A. Sen, *J. Am. Chem. Soc.*, 1996, **118**, 13111–13112.
5 (*a*) M. E. O'Reilly, R. S. Kim, S. Oh and Y. Surendranath, *ACS Cent. Sci.*, 2017, **3**, 1174–1179; (*b*) D. Xiang, J. A. Iñiguez, J. Deng, X. Guan, A. Martinez and C. Liu, *Angew. Chem., Int. Ed.*, 2021, **60**, 18152–18161; (*c*) J. Deng, *et al.*, *Nat. Commun.*, 2020, **11**, 3686.
6 M. Ahlquist, *et al.*, *J. Am. Chem. Soc.*, 2009, **131**, 17110–17115.
7 (*a*) C. J. Jones, D. Taube, V. R. Ziatdinov, R. A. Periana, R. J. Nielsen, J. Oxgaard and W. A. Goddard III, *Angew. Chem., Int. Ed.*, 2004, **43**, 4626–4629; (*b*) J. T. Fuller, S. Butler, D. Devarajan, A. Jacobs, B. G. Hashiguchi, M. M. Konnick, W. A. Goddard, J. Gonzales, R. A. Periana and D. H. Ess, *ACS Catal.*, 2016, **6**, 4312–4322; (*c*) T. R. Cundari, L. A. Snyder and A. Yoshikawa, *THEOCHEM*, 1998, **425**, 13–24; (*d*) S. Chempath and A. T. Bell, *J. Am. Chem. Soc.*, 2006, **128**, 4650–4657; (*e*) S.-S. Chen, A. Koppaka, R. A. Periana and D. H. Ess, *J. Am. Chem. Soc.*, 2021, **143**, 18242–18250.
8 R. S. Kim, A. Nazemi, T. R. Cundari and Y. Surendranath, *ACS Catal.*, 2020, **10**, 14782–14792.
9 (*a*) H. Jakob, S. Leininger, T. Lehmann, S. Jacobi and S. Gutewort, *Ullmann's Encyclopedia of Industrial Chemistry*, Wiley-VCH, Weinheim, 2012, vol. 26, p. 293; (*b*) K. Groenen Serrano, *Curr. Opin. Electrochem.*, 2021, **27**, 100679.
10 C. Madic, *et al.*, *Inorg. Chem.*, 1984, **23**, 469–476.
11 (*a*) A. B. P. Lever, *J. Chem. Educ.*, 1974, **51**, 612; (*b*) R. L. DeKock and H. B. Gray, *Chemical Structure and Bonding*, University Science Books, Mill Valley, California, 2nd edn, 1989.
12 G. L. Miessler, P. J. Fischer and D. A. Tarr, *Inorganic Chemistry*, Pearson Education, Inc., New York, 5th edn, 2014.
13 (*a*) S. E. Braslavsky, *Pure Appl. Chem.*, 2007, **79**, 293–465; (*b*) M. D. Cohen and E. Fischer, *J. Chem. Soc.*, 1962, 3044–3052.
14 J. B. Allen and R. F. Larry, *Electrochemical Methods: Fundamentals and Applications*, John Wiley & Sons, 2nd edn, 2001.
15 P. Zanello, C. Nervi and F. F. de Biani, *Inorganic Electrochemistry: Theory, Practice and Application*, RSC, Cambridge, UK, 2003.
16 J. Deng, *et al.*, *Angew. Chem., Int. Ed.*, 2021, **60**(51), 26630–26638.
17 G. Busca, *Chem. Rev.*, 2007, **107**, 5366–5410.